Sciencexpress Report

Coupling of CO_2 and Ice Sheet Stability Over Major Climate Transitions of the Last 20 Million Years

Aradhna K. Tripati,[1,2]* Christopher D. Roberts,[2] Robert A. Eagle[3]

[1]Departments of Earth and Space Sciences and Atmospheric and Oceanic Sciences, and Institute of Geophysics and Planetary Physics, University of California, Los Angeles, CA 90095, USA. [2]Department of Earth Sciences, University of Cambridge, Cambridge, CB2 3EQ, UK. [3]Division of Geological and Planetary Sciences, California Institute of Technology, Pasadena, CA 91125, USA.

*To whom correspondence should be addressed. E-mail: aradhna.tripati@gmail.com

The CO_2 content of the atmosphere has varied cyclically between ~180 and ~280 ppmv over the last 800,000 years, closely coupled with temperature and sea level. For earlier periods in Earth's history, pCO_2 is much less certain and the relationship between pCO_2 and climate remains poorly constrained. We use boron/calcium ratios in foraminifera to estimate pCO_2 during major climate transitions of the last 20 million years (myr). During the Middle Miocene, when temperatures were ~3° to 6°C warmer and sea level 25 to 40 meters higher than present, pCO_2 was similar to modern levels. Decreases in pCO_2 were synchronous with major episodes of glacial expansion during the Middle Miocene (~14 to 10 million years ago; Ma) and Late Pliocene (~3.3 to 2.4 Ma).

The response of ice sheets and climate to past and future changes in pCO_2 remains uncertain (*1*). Geologic data can be used to constrain relationships between pCO_2 and ice sheet stability, to identify climate thresholds, and to validate models used for simulating future climate change (*1*). Over the past 20 myr, there have been substantial changes in global sea level driven by the growth and decay of continental ice sheets. Among the most pronounced of these fluctuations are the growth of ice on East and West Antarctica and the formation of an Arctic ice cap in the Middle Miocene (~14 to 10 Ma), and the intensification of glaciation in the Northern Hemisphere during the Late Pliocene (~3.4 to 2.4 Ma) (*2*–*4*). The causes of these glacial transitions, however, are the subject of intense debate. Mechanisms proposed include changing ocean circulation due to the closure of the Panamanian Seaway (*5*), upper water column stratification in the tropics and/or high-latitudes [e.g., (*6*)], and orbitally-driven variations in the amount or distribution of insolation [e.g., (*2*)]. Other authors invoke pCO_2 changes to explain glacial expansion (*7*–*9*).

Although there is speculation about the role of the carbon cycle in driving these well-studied climate changes, there is surprisingly little direct evidence to support a coupling between pCO_2 and climate prior to the ice core record (i.e., before 0.8 Ma). Estimates of pCO_2 have been generated using several methods [e.g., (*10*–*13*)] including the difference in the carbon isotopic composition ($\delta^{13}C$) of alkenones and co-occurring foraminifera, $\delta^{13}C$ of bulk carbon and of pedogenic carbonates, boron isotope composition ($\delta^{11}B$) of foraminifera, stomatal density on fossil leaves, and carbon cycle modelling. Most reconstructions support a decoupling between pCO_2 (*10*–*13*) and climate (*14*) during the Miocene and Late Pliocene, although very little pCO_2 data are available and the few published proxy reconstructions yield conflicting results. In addition, few pCO_2 proxies have replicated the ice core data of the past 0.8 Ma.

To test the hypothesis that CO_2 and climate were closely coupled across these major transitions, we calculated surface water pCO_2 and pH for three intervals (20 to 5 Ma, 3.5 to 2.4 Ma, 1.4 Ma to present) using foraminiferal B/Ca ratios. Yu *et al*. demonstrated that planktic foraminiferal B/Ca ratios can be used to estimate seawater borate/bicarbonate ratios [$B(OH)_4^-/HCO_3^-$] (*15*). Seawater $B(OH)_4^-/HCO_3^-$ will respond to changes in the carbonate system (such as pH, alkalinity, or dissolved inorganic carbon) as well as the total concentration of dissolved boron. To calculate pCO_2 and pH from seawater $B(OH)_4^-/HCO_3^-$, Yu *et al*. assumed alkalinity scaled either with surface water salinity or whole ocean salinity, and total boron concentrations scaled with salinity.

We reconstructed surface water $B(OH)_4^-/HCO_3^-$ at Sites 806 and 588 located in the western tropical Pacific Ocean (fig. S1). Surface water pCO_2 at these sites should reflect atmospheric pCO_2, as today this region is close to equilibrium with the atmosphere (table S2), is not strongly affected by upwelling, and is characterized by low productivity. Although ocean stratification has likely changed over the past 20 myr, the western tropical Pacific probably experienced much smaller fluctuations than other regions (the eastern sides of ocean basins; mid-latitude settings; high-latitude settings) (*6*, *16*, *17*). Surface temperatures in this region are also thought to have been relatively stable over long timescales (*18*, *19*), with fluctuations of <6°C, in contrast to other areas (*16*, *17*). Both sites were drilled in shallow waters (table S1), with well-preserved planktonic foraminifera (*10*, *17–20*).

We measured B/Ca ratios, Mg/Ca ratios, and $\delta^{18}O$ values in mono-specific samples of the surface-dwelling species *Globigerinoides ruber* and *G. sacculifer* (tables S3 and S4). Average reproducibility for B/Ca ratios of separately cleaned samples was 3.5%. B/Ca ratios were converted to seawater $B(OH)_4^-/HCO_3^-$ ratios using an appropriate value for K_D. K_D was calculated for each sample by applying a species-specific K_D-temperature calibration (table S7) to Mg/Ca-derived estimates of temperature. Calculated $B(OH)_4^-/HCO_3^-$ ratios (and pCO_2 values) for 20 replicates typically differ by less than 4% (table S8), and values calculated using 78 pairs of *G. ruber* and *G. sacculifer* from the same sample agreed to within 3%, on average (table S9). Materials and methods are available as supporting material on *Science* Online.

In order to estimate pH and pCO_2 from $B(OH)_4^-/HCO_3^-$ ratios, a further assumption is required to fully constrain the carbonate system. We use seawater $B(OH)_4^-/HCO_3^-$ ratios and estimates of alkalinity or carbonate ion concentration to determine pH and pCO_2 (Section F of supporting material). We tested the sensitivity of calculated pH and pCO_2 values to the assumption used, including assuming: (i) alkalinity scaled with salinity (blue circles in Figs. 1 and 2), (ii) constant carbonate ion concentration, and (iii) variable carbonate ion concentration. Changes in seawater B also were considered, as it has an oceanic residence time of ~11 to 17 myr (*21*). We assumed total B (fig. S7) scaled with salinity or followed modelled histories (*21*). Equations used for our calculations are listed in Sections G to I of supporting material.

In total, we used 28 different sets of models to calculate pH and pCO_2 from $B(OH)_4^-/HCO_3^-$ ratios (figs. S5 to S8 and table S12). The range of calculated values defines the shaded regions in Figs. 1 and 2. pCO_2 values calculated using the 28 models agree to within 40 ppmv over the last 800 kyr, with the difference between minimum and maximum calculated values increasing farther back in time (50 ppmv from 0 to 5 Ma, 60 ppmv from 5 to 10 Ma, and 100 ppmv from 10 to 20 Ma).

The pCO_2 reconstruction accurately reproduces ice core measurements from 0 to 0.8 Ma (Fig. 1). If the variable alkalinity model is considered (Fig. 1, blue circles), ~30 to 50 ppmv offsets are observed for 3 (of 41) samples, which may be due to differences in age models (128 and 374 Ka) or inaccuracies in the reconstruction (at 581 Ka). For the whole population of pCO_2 estimates from this interval ($n = 39$), the root mean square error of the residuals (between observed pCO_2 values from ice cores and reconstructed pCO_2 from foraminiferal B/Ca using the variable alkalinity model) is 13 ppmv (fig. S9). If the other 26 models are considered, then all 41 values lie within error of the ice core record. Although only moderate in resolution, our record shows the change in the amplitude of the 100 kyr cycle at 650 Ka seen in ice cores (*22*). We also reproduce the trends over the past 1.4 Ma observed in a recently published $\delta^{11}B$ record (*11*).

Results for the Miocene and Late Pliocene support a close coupling between pCO_2 and climate (Fig. 2). Relative to today, surface waters appear to have been more acidic, and pCO_2 values higher (Fig. 2, A and B), during the Early and Mid-Miocene (~20 to 15 Ma). This interval was characterized by global warmth, with little evidence for substantial (i.e., similar to modern) ice storage on Antarctica or Greenland (*3*, *14*, *23*). The highest estimates of pCO_2 occur during the Mid-Miocene Climatic Optimum (MMCO; ~16 to 14 Ma), the only interval in our record with levels higher than the 2009 value of 387 ppmv. Climate proxies indicate the MMCO was associated with reduced ice volume and globally higher sea level (25 to 40 meters) (*3*), as well as warmer surface and deep-water temperatures (*2*, *20*). These results are consistent with foraminiferal $\delta^{11}B$ data that indicate surface waters were more acidic ~20 Ma (*12*).

Following the MMCO in the Mid-Miocene (~14 to 10 Ma), surface water pH increased and pCO_2 decreased by ~200 ppmv. This pattern mirrors long-term trends in $\delta^{18}O$ records and is correlated with the appearance and growth of ice in both hemispheres, consistent with CO_2 driving this transition. Global cooling appears to have begun at ~14.2 Ma (*2*), and subsequent glacial expansion drove an 0.7 to 1.0‰ increase in seawater and benthic foraminiferal $\delta^{18}O$ (*24*) and a lowering of sea level (~40 ± 15 meters) (*3*). In the Northern Hemisphere, this fall in pCO_2 coincides with the onset of perennial Arctic sea ice cover (*25*), the development of substantial ice storage (*14*), and the first Miocene occurrence of ice-rafted debris (IRD) in the North Atlantic, indicating glaciers reached sea level (*23*). In the Southern Hemisphere, decreasing pCO_2 is associated with the change from wet- to cold-based alpine glaciers in the McMurdo Dry Valleys (*26*), transition to cold polar conditions and the growth of ice on West Antarctica (*27*), and reinitiation of a large ice sheet on East Antarctica (*2*, *28*).

During the Late Miocene (~10 to 7 Ma), seawater pH was relatively high, and pCO_2 low and stable (~220 ppmv). Small ice sheets on West Antarctica and in the Northern Hemisphere are thought to have expanded while temperatures cooled (*13*). In the latest Miocene (~7 to 5 Ma), pH and pCO_2 exhibit large-amplitude variations, although the trends are poorly defined. This interval has been interpreted as generally being warm, with interglacials representing complete deglaciation of marine-based regions of Antarctica (*29*), consistent with the limited data on our pCO_2 curve.

Our B/Ca record indicates a large increase in pH and fall in pCO_2 (~150 ppmv) during the Late Pliocene (~3.4 to 2.4 Ma) (Fig. 2, C and D). This evidence for a decline in pCO_2

coincident with the intensification of glaciation is consistent with the hypothesis that pCO_2 was the major driver of ice growth at this time. Model simulations also support the idea that changing pCO_2, and not ocean heat transport, triggered glaciation (*30*). Comparison with other records indicates decreasing pCO_2 is synchronous with the intensification of continental glaciation in the Northern and Southern Hemispheres, as indicated by increased foraminiferal $\delta^{18}O$ (*31*), the onset of ice-rafting in the North Pacific, and increased rates of ice-rafting in the North Atlantic (*23*, *32*) and Southern Ocean (*33*). In addition, the interval of low pCO_2 at ~2.5 Ma is associated with the onset of large amplitude (glacial-interglacial) cycles in deep-sea oxygen isotope records (*31*).

These results show that changes in pCO_2 and climate have been coupled during major glacial transitions of the past 20 myr, just as they have been over the last 0.8 myr, supporting the hypothesis that greenhouse gas forcing was an important modulator of climate over this interval via direct and indirect effects. Variations in pCO_2 affect the radiative budget and energy balance of the planet. Such changes will inevitably have consequences for temperature, the hydrologic cycle, heat transport, and the accumulation and ablation of sea ice and glacial ice. The data presented do not preclude alternative mechanisms for driving climate change over the past 20 Ma; however, they do indicate changes in pCO_2 were closely tied to the evolution of climate during the Middle and Late Miocene, and Late Pliocene glacial intensification, and therefore it is logical to deduce pCO_2 played an important role in driving these transitions. High-resolution records of pCO_2 and other climate parameters should help to resolve whether pCO_2 was a trigger and/or feedback (or both).

These results provide some constraints on pCO_2 thresholds for the advance and retreat of continental ice sheets in the past, which is also relevant in the context of anthropogenic climate change since it is uncertain how continental ice sheets will respond over the coming centuries to increased levels of pCO_2 (*1*). By comparing our reconstruction to the published datasets described above, we are able to estimate past thresholds for the build up of ice in different regions. When pCO_2 levels were last similar to modern values (greater than 350 to 400 ppmv), there was little glacial ice on land, or sea ice in the Arctic, and a marine-based ice mass on Antarctica was not viable. A sea-ice cap on the Arctic Ocean and large permanent ice sheet was maintained on East Antarctica when pCO_2 values fell below this threshold. Lower levels were necessary for the growth of large ice masses on West Antarctica (~250 to 300 ppmv) and Greenland (~220 to 260 ppmv). These values are lower than indicated by a recent modelling study, which suggested the threshold on East Antarctica may have been 3× greater than in the Northern Hemisphere (*34*).

This work may support a relatively high climate sensitivity to pCO_2. pCO_2 values associated with major climate transitions of the past 20 Ma are similar to modern levels. During the Mid-Miocene, when pCO_2 was apparently grossly similar to modern levels, global surface temperatures were on average 3 to 6°C warmer than present (*2*, *24*). We suggest the Mid-Miocene would be useful to study in order to understand what effect sustained high pCO_2 levels (i.e., a climate in equilibrium with near-modern pCO_2 values) may have on climate.

References and Notes

1. IPCC, Climate Change 2007: The Physical Science Basis. Contribution of Working Group I to the Fourth Assessment Report of the Intergovermental Panel on Climate Change, S. Solomon et al., Eds. (Cambridge Univ. Press, Cambridge, 2007), p. 996.
2. A. Shevenell, J. Kennett, D. Lea, Science **305**, 1766 (2004).
3. K. Miller et al., Science **310**, 1293 (2005).
4. G. Haug, D. Sigman, R. Tiedemann, T. Pedersen, M. Sarnthein, Nature **401**, 779 (1999).
5. G. Haug, R. Tiedemann, Nature **393**, 673 (1998).
6. D. Sigman, S. Jaccard, G. Haug, Nature **428**, 59 (2004).
7. E. Vincent, W. Berger, in The Carbon Cycle and Atmospheric CO_2: Natural Variations Archean to Present, E. Sundquist, W. Broecker, Eds. (Geophys. Monogr. Ser., AGU, Washington, DC, 1985), vol. 32, pp. 455–468.
8. A. Holbourn, W. Kuhnt, M. Schulz, H. Erlenkeuser, Nature **438**, doi:10.1038/nature04123 (2005).
9. D. Hodell, F. Woodruff, Paleoceanography **9**, 405 (1994).
10. M. Pagani, J. Zachos, K. Freeman, B. Tipple, S. Bohaty, Science **309**, 600 (2005).
11. B. Hoenisch, N. Hemming, D. Archer, M. Siddall, J. McManus, Science **324**, 1551 (2009).
12. A. Spivack, C. You, H. Smith, Nature **363**, 149 (1993).
13. P. Pearson, M. Palmer, Nature **406**, 695 (2000).
14. J. Zachos, M. Pagani, L. Sloan, E. Thomas, K. Billups, Science **292**, 686 (2001).
15. J. Yu, H. Elderfield, B. Hoenisch, Paleoceanography **22**, doi:10.1029/2006PA001347 (2007).
16. A. Federov et al., Science **312**, 1437 (2006).
17. M. Wara, A. Ravelo, M. Delaney, Science **309**, 758 (2005).
18. S. Nathan, R. Leckie, Palaeogeogr. Palaeoclimatol. Palaeocecol. **274**, 140 (2009).
19. M. Medina-Elizalde, D. Lea, Science, doi:10.1126/science.1115933 (2005).
20. B. Flower, J. Kennett, Paleoceanography **8**, 811 (1993).
21. D. Lemarchand, J. Gaillardet, E. Lewin, C. Allegre, Chem. Geol. **190**, 123 (2002).
22. D. Luthi et al., Nature **453**, 379 (2008).

23. T. Wolf-Welling, M. Cremer, S. O'Connell, A. Winkler, J. Thiede, in Proceedings of Ocean Drilling Program, Scientific Results, J. Thiede, A. Myhre, J. Firth, G. Johnson, W. Ruddiman, Eds. (College Station, TX, 1996), vol. 151, pp. 515–568.
24. K. Billups, D. Schrag, Earth Planet. Sci. Lett. **209**, 181 (2003).
25. A. Krylov et al., Paleoceanography **23**, doi:10.1029/2007PA001497 (2008).
26. A. Lewis et al., PNAS **105**, 10676 (2008).
27. T. Naish et al., Nature **458**, 322 (2009).
28. B. Flower, J. Kennett, Paleoceanography **10**, 1095 (1995).
29. T. Naish et al., in ISAES (Santa Barbara, 2007).
30. D. Lunt, G. Foster, A. Haywood, E. Stone, Nature **454**, 1102 (2008).
31. L. Lisiecki, M. Raymo, Paleoceanography **20**, doi:10.1029/2004PA001071 (2005).
32. L. Krissek, in Proc. ODP, Sci. Results, D. Rea, I. Basov, D. Scholl, J. Allan, Eds. (Ocean Drilling Program, College Station, TX, 1995), vol. 145, pp. 179–194.
33. E. Cowan, in Proceedings of the Ocean Drilling Program, Scientific Results, P. Barker, A. Camerlenghi, G. Acton, Eds. (College Station, TX, 2001), vol. 178, pp. 1–22.
34. R. DeConto et al., Nature **455**, 652 (2008).

35. We would like to express our appreciation to K. Caldeira, H. Elderfield, J. Eiler, T. Naish, D. Sigman, anonymous reviewers, and the editor for their comments on this work, which substantially improved the manuscript. We also would like to thank J. Booth, E. Khadun, O. Shorttle, L. Thanalasundaram, and A. Bufe for invaluable assistance with sample preparation; L. Booth, J. Day, and M. Greaves (supported on NE/F004966/1) for technical assistance; L. Lisiecki for assistance with the age model; and S. Crowhurst, A. Gagnon, S. John, N. Meckler, B. Passey, N. Thiagarajan, and J. Yu for discussing this work. Support was provided to A.K.T. by UCLA, NERC (NE/D009049/1), and Magdalene College; to C.D.R. by NERC (NER/S/A/2006/14070); and to R.A.E. by a Caltech Chancellors Postdoctoral Scholarship. Samples for this study were obtained from the Godwin Laboratory sample archives and the Ocean Drilling Program.

Supporting Online Material

www.sciencemag.org/cgi/content/full/1178296/DC1
Materials and Methods
Figs. S1 to S9
Tables S1 to S12
References

26 June 2009; accepted 28 September 2009
Published online 8 October 2009; 10.1126/science.1178296
Include this information when citing this paper.

Fig. 1. $B(OH)_4^-/HCO_3^-$ ratios, pH, and pCO_2 from 0 to 1.4 Ma from B/Ca ratios of surface-dwelling foraminifera compared to Antarctic ice core data (solid line) (*22*). Data are mean ± average σ. There is a 3.5% analytical uncertainty in B/Ca ratios (average 1σ) based on analyses of replicate samples (table S8), and a 4% uncertainty in reconstructed seawater $B(OH)_4^-/HCO_3^-$ ratios based on 78 paired measurements of *G. ruber* and *G. sacculifer* (table S9). This uncertainty in $B(OH)_4^-/HCO_3^-$ equates to a 10 to 20 ppmv uncertainty (1σ) in pCO_2 (~5 to 6%), and a 0.02 uncertainty in pH (~0.2%). Gray shaded region brackets all calculated pCO_2 values. Blue circles assume alkalinity and total boron scale with salinity. Vertical dashed lines on left show Early-Mid Pleistocene and Mid-Late Pleistocene boundaries. Horizontal solid and dashed lines approximately mark shifts in mean and amplitude of values. For comparison, $\delta^{11}B$-based pCO_2 estimates indicate pCO_2 of ~220 to 300 ppmv from 0.8 to 1.4 Ma (*11*).

Fig. 2. pCO_2 for Miocene and Late Pliocene from B/Ca ratios of surface-dwelling foraminifera compared to climate records. Error bars are same as in Fig. 1. Gray shaded region brackets all calculated pCO_2 values. Blue circles assume alkalinity and total boron scale with salinity. (**A**) $B(OH)_4^-/HCO_3^-$ ratios and pH for 20 to 5 Ma. (**B**) pCO_2 and compilation of benthic foraminiferal $\delta^{18}O$ (*14*) for 20 to 5 Ma. Marked at bottom by numbered bars is timing of 1: the Mid-Miocene Climatic Optimum (*2*, *3*, *14*, *20*, *23*), 2: Mid-Miocene glacial expansion (*2*, *3*, *8*, *14*, *23*–*28*). (**C**) $B(OH)_4^-/HCO_3^-$ ratios and pH for 3.4 to 2.4 Ma. (**D**) pCO_2 and benthic foraminiferal $\delta^{18}O$ (*31*) for 3.4 to 2.4 Ma. Marked at the bottom by dark blue bar is reported timing of Late Pliocene glacial expansion (*14*, *23*, *31*–*33*).

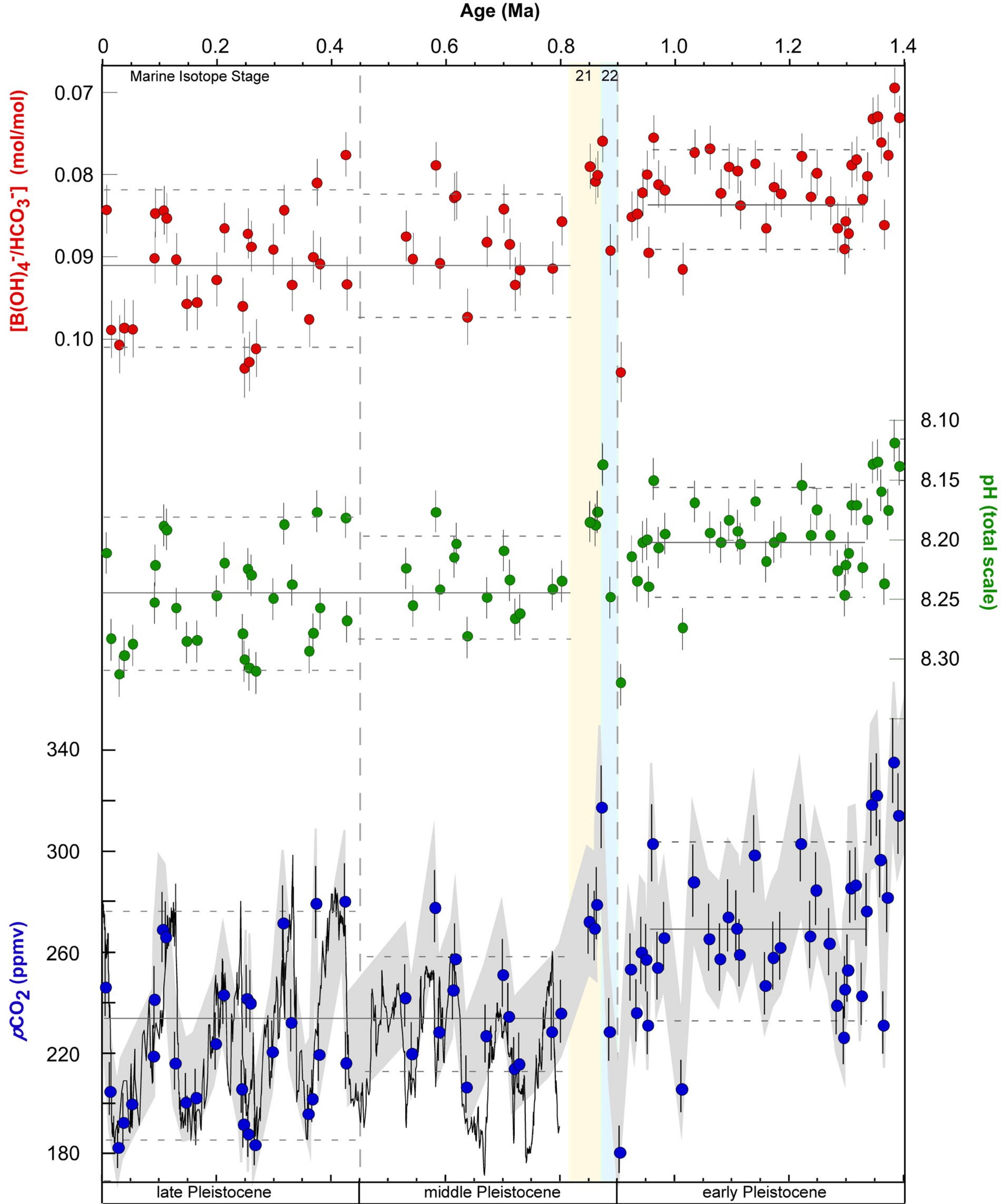
Age (Ma)
0
0.2
0.4
0.6
0.8
1.0
1.2
1.4
Marine Isotope Stage
21
22
$[B(OH)_4^-/HCO_3^-]$ (mol/mol)
0.07
0.08
0.09
0.10
pH (total scale)
8.10
8.15
8.20
8.25
8.30
pCO_2 (ppmv)
340
300
260
220
180
late Pleistocene
middle Pleistocene
early Pleistocene

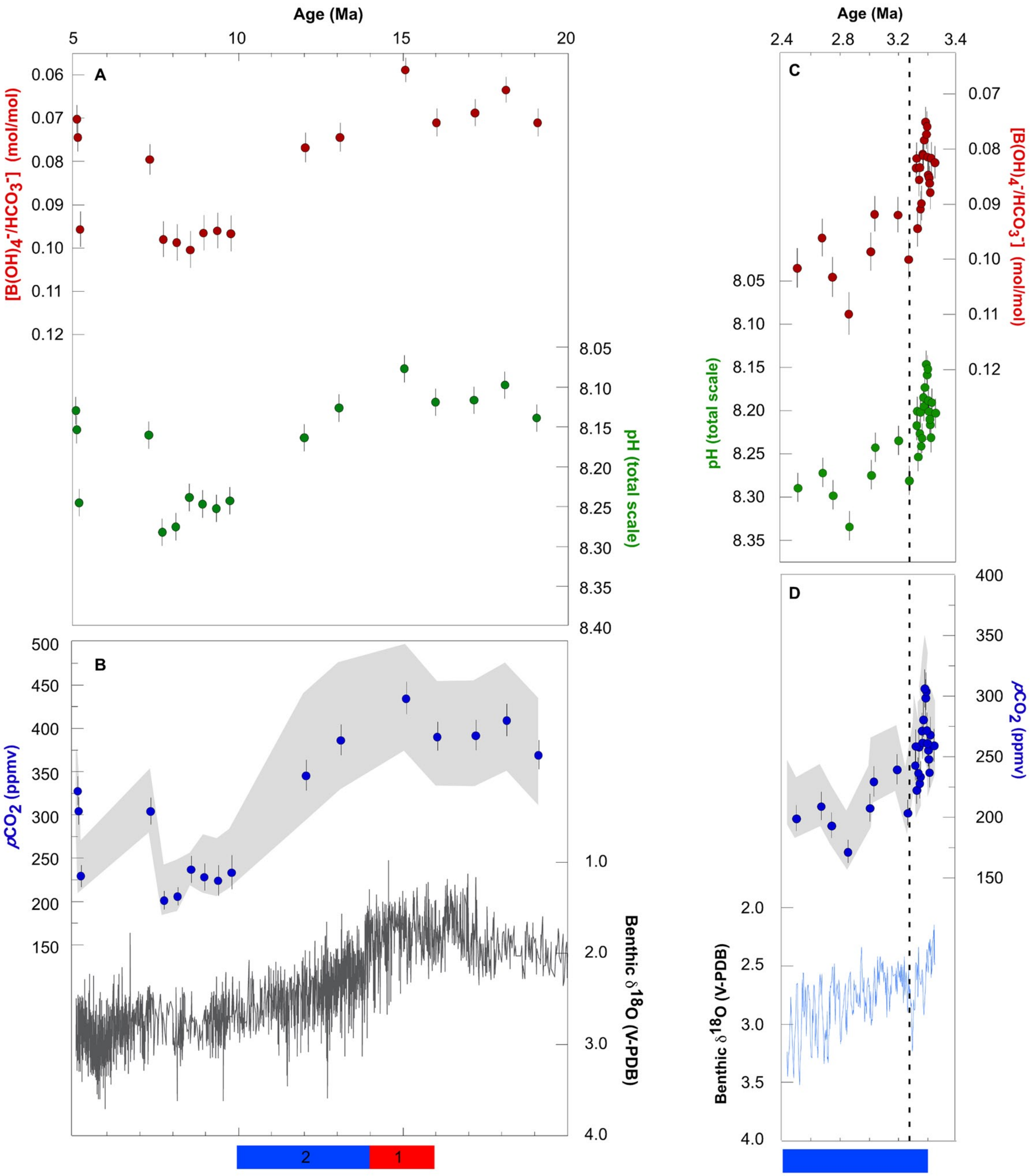
Age (Ma)
5
10
15
20
A
[B(OH)$_4^-$/HCO$_3^-$] (mol/mol)
0.06
0.07
0.08
0.09
0.10
0.11
0.12
pH (total scale)
8.05
8.10
8.15
8.20
8.25
8.30
8.35
8.40
B
pCO$_2$ (ppmv)
500
450
400
350
300
250
200
150
Benthic δ^{18}O (V-PDB)
1.0
2.0
3.0
4.0
2
1
Age (Ma)
2.4
2.6
2.8
3.0
3.2
3.4
C
[B(OH)$_4^-$/HCO$_3^-$] (mol/mol)
0.07
0.08
0.09
0.10
0.11
0.12
pH (total scale)
8.05
8.10
8.15
8.20
8.25
8.30
8.35
D
pCO$_2$ (ppmv)
400
350
300
250
200
150
Benthic δ^{18}O (V-PDB)
2.0
2.5
3.0
3.5
4.0